(Received 6 July 2024, Accepted 5 November 2024, Scheduled 19 November 2024)

Design of F-Shaped Parasitic MIMO Antenna with DGS for Vehicle-to-Everything Communication

Maruti R. Jadhav* and Uttam L. Bombale

Electronics Engineering, Shivaji University, Vidya Nagar, Kolhapur, Maharashtra 416004, India

ABSTRACT: Multiple-Input Multiple-Output (MIMO) antennas are essential for transmitting and receiving information in Vehicle to Everything (V2X) communication. However, the MIMO antenna designs at V2X are complex because of the mutual coupling problem. Several approaches have been designed to improve antenna isolation. However, these approaches have drawbacks like gain, bandwidth, and radiation efficiency reductions. This work introduces a compact four-port MIMO antenna that operates at a 5.85 GHz to 5.9 GHz frequency range for V2X communication. Here, the slotted circular microstrip patch MIMO antenna is considered. The antenna's length, width, and patch are optimized by metaheuristic optimization called Aquila Optimization (AO). A substrate Rogers RT5880, which has a defected ground structure (DGS) and a parasitic patch, is used to design the antenna. F-shaped parasitic elements are placed near each antenna element to improve isolation. The DGS with a U-shaped parasitic element minimizes the mutual coupling among the adjacent antenna elements. The considered overall dimension has a compact size, and it achieves better envelope correlation coefficient (ECC < 0.5), total active reflection coefficient (TARC < -10 dB), diversity gain (DG > 9.9 dB), channel capacity loss (CCL < 0.4), and mean effective gain (MEG < 3 dB) at 5.88 GHz. Hence, it is proposed that the developed design is useful for applying V2X communications.

1. INTRODUCTION

An antenna is essential to communication systems and transmits the signal into free space. In traditional communication systems, the single antenna was utilized at both the transmitter and receiver. This type of communication model is called single input single output (SISO) [1, 2]. This SISO model is simple and easy to design; however, it is susceptible to the issues caused by multi-path effects. Multiple-input multiple-output (MIMO) designs are introduced to tackle this issue [35]. MIMO technology uses antennas at the transmitter and receiver sides [3]. Currently, antenna engineers focus on the MIMO antenna because of its capacity to transmit a multi-identical signal with less correlation to the fading environment [36, 37]. This characteristic enhances the communication systems' stability, reliability, and channel capacity [4].

Vehicle-to-everything (V2X) communications have gained a lot of attention in various countries and are major for intelligent transportation. V2X communication has two communications, namely, Vehicle to Vehicle (V2V) and Vehicle to infrastructure (V2I) [5]. This communication depends on the Dedicated Short-Range Communications (DSRCs) and operates with the range of 5.85 to 5.925 GHz frequency bands for information transfer. V2X makes vehicles for communication among the environment, vehicles, and traffic using short region wireless signal. One of the major applications of V2X is to allocate information on position and velocity to alert other drivers regarding potential hazards [6–8]. For V2X communication system, circularly polarized (CP) MIMO antennas are the best solution over linear polarization (LP). CP has various advantages over LP based on signal propagation. CP MIMO antennas communicate in two orthogonal positions, and it has several advantages over LP antennas in terms of fading, interference, and multipath distortion. Hence, CP is widely utilized in 5G, satellite, device-to-device (D2D), and wireless communications [9, 10].

In MIMO system, placing multi-antennas in a miniaturized space is complex, and mutual coupling occurs [39]. This coupling happens due to the interconnection of radiation from the antenna elements and surface current flow on the ground [11, 12]. This coupling minimizes the diversity performance and minimizes the isolation among nearby antennas [41, 42]. Several approaches have been analysed to suppress mutual coupling and enhance isolation. Evaluating the antennas' surface current is one way to determine the mutual coupling. Further, some research works use decouplers, neutralization lines, orthogonal polarization, and parasitic elements to reduce the coupling [13–15]. Further, methods like defected ground structure (DGS), polarization diversity, and electromagnetic band gap (EBG) are also used to drop the coupling. Another approach, band-stop filter and slit ring resonators (SRRs) reduce the coupling [16–18].

2. MOTIVATION

The recent need for wireless communication requires large data rates with effective spectrum management exploiting multi-antennas. MIMO antenna provides data transmission across multiple streams by using multiple antennas at both transmission and receiver ends. In existing research, various MIMO

* Corresponding author: Maruti R. Jadhav (maruti.jadhavdte@gmail.com).

antennas like PIEA, planar LTE, etc. were developed for V2X communication. However, these antenna models have some issues like close placement of antenna which lead to electromagnetic interactions, poor isolation, and signal degradation issues due to mutual coupling issues. This mutual coupling causes reduced data rates, lower channel capacity and reduced gain and efficiency. In order to overcome these existing issues, U-shaped DGS and F-shaped parasitic stubs have been used in the antenna design to enhance efficiency and reduce mutual coupling issues. Hence, this research work focuses on the design of a MIMO antenna for V2X communication with DGS and F-shaped parasitic elements. The major objectives of the research work are:

- To introduce a compact four-port circular-shape MIMO antenna for vehicle to everything (V2X) communication.
- To introduce an enhanced metaheuristic optimization for optimizing the dimensions of the antennas.
- To introduce defected ground structure (DGS) and F-shaped parasitic elements to minimize mutual coupling among the adjacent antennas.

3. RELATED WORKS

Certain recent research works related to MIMO antenna design for applications like V2X communication, 5G, WiMAX, and WLAN are presented in this section.

Sujanth Narayan et al. [18] introduced a co-planar waveguide (CPW) with a MIMO antenna for V2X communication. This antenna was designed with 2 rectangular patches and slots and resonated at two frequencies (3.5 GHz, 5.9 GHz). This design achieved a reflection coefficient of < -10 dB and a voltage standing wave ratio (VSWR) of less than two, and the efficiency was achieved between 60% and 80% for both frequency ranges. Ishfaq et al. [19] described a new compact planar inverted E antenna (PIEA) for V2X application. This system was designed with a 4×4 Butler-matrix (BM) with the spacing of $0.3\lambda_0$. Based on a cross-coupled crossover, Butler matrix was designed without phase shifters, which utilizes microstrip couplers and crossover planes in planar structure.

Sufian et al. [20] introduced a four-port CP-MIMO antenna that operates at 5.9 GHz for V2X communication, in which circular-shape parasites with DGS were utilized to minimize mutual coupling. Here, the overall dimension of the antenna was 32 mm $\times$ 52 mm. The simulation and fabrication results showed that this proposed design provided an axial ratio of 3 dB, an overlapping S_{11} of -10 dB, and achieved better gain.

Ko et al. [21] designed a planar LTE with a sub-6 GHz-based MIMO antenna to apply V2X communication. In this design, miniaturization was attained by inter-digital and gap capacitors. Here, the antenna was designed with Taconic TLY 5 substrate material with thickness of 0.254 mm. This model has obtained isolation values of 21 dB for the resonating frequency range from 24 GHz to 36 GHz. The measured antenna achieved 0.8 to 1.9 GHz, 2.3 to 5.1 GHz, and 1.1 dB gain for LTE with sub-6 GHz, 28.2 to 31 GHz, 33 to 34 GHz, and 10.9 dB for 5G communication.

Ali et al. [22] developed a 4×4 MIMO antenna for WLAN and Wi-MAX applications. This design has 4 slot radiators transverse to each other. To provide the switching capacity of dual modes, 4 metal strips were inserted into the resonators. This model achieved less ECC value of 0.002 and DG of 10 dB. The performances such as reflection coefficient, insertion loss, radiation pattern, and gain plot were evaluated for this approach.

Dwivedi et al. [23] introduced a two-port CP-MIMO antenna to apply 5G in 6 GHz band. The shape of the antenna was a T-shaped radiator with a rectangle ring shape ground plane placed opposite to each other. This design has an impedance bandwidth of 900 MHz, and the isolation among the elements was less than -15 dB. Further, this model achieved a radiation efficiency of 95%. This model achieved a lower envelope correlation coefficient (ECC) value of 0.10 and a DG of 9.9 dB. Naidu et al. [24] introduced a maze-shaped asymmetric co-planar strip (ACS) with MIMO for V2V and WiMaX communications. This design was simulated on an FR-4 substrate and operated with an average isolation of 20 dB. This model achieved an efficiency of 88%, ECC was less than 0.001; DG was 9.94 dB; and the minimum isolation achieved was -18 dB.

Sharma et al. [25] suggested a leaf clover shaped MIMO antenna for sub-6 GHz V2X applications, which was operated at various bands like WiMAX, WiLAN, etc. Here, the antenna was designed with the dimension of 60 $\times$ 40 $\times$ 0.256 mm^3. This model has reached improved gain values for the same operating frequency ranges. Aliqab et al. [26] suggested a highly decoupled two-port MIMO antenna for V2X communication, which was operated at frequency range of 5.85 GHz to 5.95 GHz. The antenna was designed on a flexible polymide substrate with the thickness of 0.6 mm, which has the total dimension of 60 $\times$ 87 mm^2. This antenna model has achieved high radiation efficiency of 95% and ECC of less than 0.001. The performances such as S-parameters, radiation pattern, gain, and efficiency were evaluated for this model.

In various existing researches, DGS, parasitic elements, slots, and stubs were added to antenna designs to reduce mutual coupling issues.

4. PROPOSED ANTENNA GEOMETRY

The geometry of 2×2 and 4×4 MIMO antennae is considered in this work. The antenna patch is a square patch, and it is made by $\lambda/4$ feedline and 50 Ω microstrip line. In this work, the substrate used is Rogers RT5880, and it has the dielectric constant $\in_r$ and loss tangent $\tan\delta$ values of 2.2 and 0.0013. Here, U-shaped DDS is designed to reduce the antenna size and minimize cross-polar radiations. Further, an F-shaped parasitic element is placed among the 4-ports to reduce the mutual coupling. The width of the patch is computed by:

$$W = \frac{c_0}{2F_r}\sqrt{\frac{2}{\varepsilon_r + 1}} \tag{1}$$

where F_r and c_0 are the resonant frequency and velocity.

R_a (radius) of the slotted circular microstrip patch MIMO antenna is computed by:

$$R_a = \frac{F}{\left(1+\frac{2h}{\pi\varepsilon_r F\left[\ln\left(\frac{F\pi}{2h}\right)+1.7726\right]}\right)^{1/2}} \quad (2)$$

$$F = \frac{8.791\times10^9}{F_r\sqrt{\varepsilon_r}} \quad (3)$$

where h is the substrate height.

Initially, the dimensions of an antenna are computed using the above expressions. Then, parameters like length, width, and patch of the antenna are optimized using Aquila Optimization (AO) [27]. The major aim of optimization is to identify the best set of values. For designing the 4 port MIMO antenna for V2X communication at the frequency of 5.82 GHz, the fitness function focuses on minimizing the return loss (S_{11}) and maximizing the gain (G) of an antenna. The fitness function is given as follows:

$$fitness = \max(G) + \min(S_{11}) \quad (4)$$

In AO, initially, the population Y begins with randomly created values in the upper and lower bounds, and it is given as:

$$Y_{kl} = rand \times (UL_l - LL_l) + LL_l \quad (5)$$

where Y_{kl} is the lth position of the kth solution, and UL_l and LL_l are the upper and lower limits of lth position.

The characteristics, such as the selection of large glides, searching the area with vertical slopes, low glide attack and exploration, low flight exploitation, and fetching prey using the foot, are discussed in the following section.

Stage 1: Y_1 — Expanded exploration

In this stage, Aquila identifies the hunting region and selects the best hunting area with a large glide-searching area and a vertical slope. It is mathematically given as:

$$Y_1(t+1) = Y_b(t)\left(1-\frac{t}{T}\right) + (Y_M(t) - Y_b(t) \times rand) \quad (6)$$

where $Y_1(t+1)$ is the solution of $(t+1)$th iteration, $Y_b(t)$ the best solution attained at tth iteration, and $Y_M(t)$ the average value of existing solutions positions at the tth iteration.

Stage 1: Y_2 — Short exploration

In this stage, the hunting region is identified with the large flight. In low glide attack and exploration, the Aquila makes the attacking field by making circles on the prey, and it is given as:

$$Y_2(t+1) = Y_b(t) \times Levy() + +Y_R(t) - (z-y) \times rand \quad (7)$$

where $Y_2(t+1)$ is the result of $(t+1)$th iteration, $Y_R(t)$ the random solution, and $Levy()$ the distribution of Levy's flight.

Stage 3: Y_3 — Expanded exploitation

In this stage, when the prey region is exactly identified, and the Aquila tries to land an attack, it will abruptly advance towards the prey. It is expressed mathematically as:

$$Y_3(t+1) = Y_b(t) - Y_M(t) \times \beta - rand + ((UL - LL)rand + LL) \times \delta \quad (8)$$

where $Y_3(t+1)$ is the solution of $(t+1)$th iteration, and β and δ are the variables used to tune the exploitation.

Stage 4: Y_3 — Short exploitation

In this stage, the Aquila attacks the prey based on stochastic characteristics and is known as catching and walking prey. It is described as:

$$Y_4(t+1) = Q_F \times Y_b(t) - (H_1 \times Y(t) \times rand) + (H_2 \times Levy() + rand \times H_1 \quad (9)$$

where $Y_4(t+1)$ is the result of $(t+1)$th iteration; Q_F is the quality function; H_1 and H_2 are the AO's movement and slope of the flight.

Figures 1(a)–(d) define the configurations of the 4-port and 2-port MIMO antennas, U-shaped DGS, and F-shaped parasitic patch. Figure 1(a) represents the overall proposed antenna model with F-shaped stubs and U-shaped DGS. Here, the substrate length and width are $a = 73.2$ mm, $b = 73.3$ mm; extra spacing of feedline and patch is mentioned in $c = 6.13$ mm, $d = 4$ mm, $e = 4.85$ mm. The length of the feedline is $f = 23$ mm, and the radius of the patch is $r = 9$ mm. For F-shaped parasitic stubs, design parameters are described as follows: $a = 26.25$ mm, $b = 13.125$ mm, $c = 9.625$ mm, and $d = 3.5$ mm. The optimized antenna parameters are represented in Table 1. Figure 2 shows the equivalent circuit of the MIMO antenna design.

TABLE 1. Optimized antenna parameters.

Parameters	Values	
	Before optimization	After optimization
Substrate length	71	73.2
Substrate height	71.1	73.3
Patch radius	8	9

5. RESULTS ANALYSIS

Some of the experimental details, algorithm, software tools used for simulation and analysis are represented Table 2.

The developed 4-port antenna with DGS and a parasitic patch is presented in this section. The overall design is demonstrated in HFSS and MATLAB platforms. The metrics like return loss, voltage standing wave ratio (VSWR), and transmission coefficient are measured. Finally, compatibility of the suggested 4 port MIMO system in 5G application is evaluated based on diversity performances like envelope correlation coefficient (ECC), diversity gain (DG), total active reflection coefficient (TARC), mean effective gain (MEG), and channel capacity loss (CCL).

Return loss: It is also called as S_{11} parameter, and it is the measurement of reflected wave that returns back to the transmitter from the antenna. The range of return loss must be less than -10 dB for a better design. Figure 3 represents the return loss of 4 ports, 2 ports, with and without parasitic element and with and without DGS, measured and simulated and parametric analysis. The return loss of the proposed antenna with DGS is 16.5 dB at 5.88 GHz; without DGS, a very low

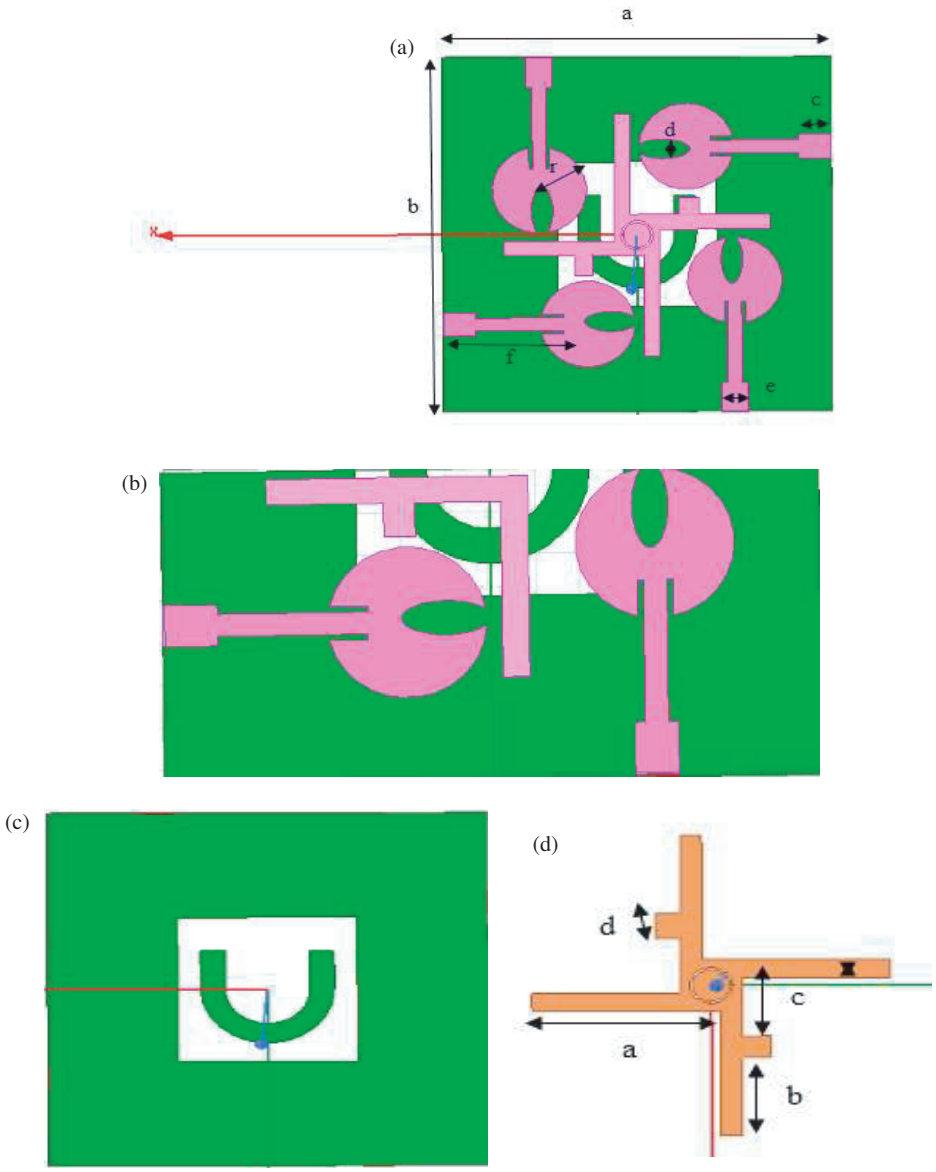

FIGURE 1. Configuration of (a) 4 port MIMO antenna, (b) 2 port MIMO antenna, (c) U-shaped DGS, (d) F-shaped parasitic patch.

TABLE 2. Experimental and algorithm details.

Parameters	Descriptions
Vector network analyzer (VNA)	Agilent N5247A: A.09.90.02
Calibration Kit	3.5 SMA calibration kit.
Optimization algorithm	Aquila optimization
Software implementation of optimization	MATLAB
Tool	HFSS
Operating frequency	2 GHz–8 GHz

return loss of −8 dB is achieved. This shows that DGS is essential for the MIMO antenna and is suitable for V2X communication. Figure 3(a) shows the return losses of 4 ports and 2 ports. The return losses of 4 port and 2 port antennas at resonating frequency are −16 dB and −19 dB, respectively. Figure 3(b) shows the proposed antenna design and antenna without parasitic elements. The return loss of the proposed design is −16 dB, and the antenna without parasitic elements resonates at −22 dB. Figure 3(c) shows the return loss of the proposed antenna with DGS and without DGS. The return loss with DGS is −17 dB and without DGS is −8 dB. Figure 3(d) shows the

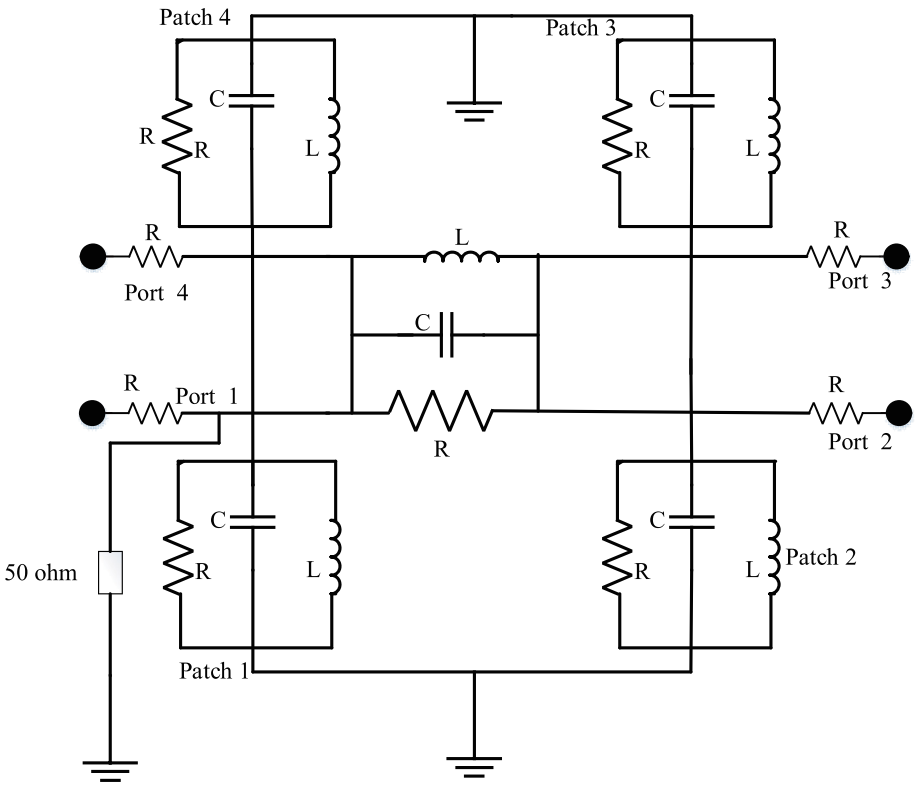

FIGURE 2. Equivalent circuit of MIMO antenna.

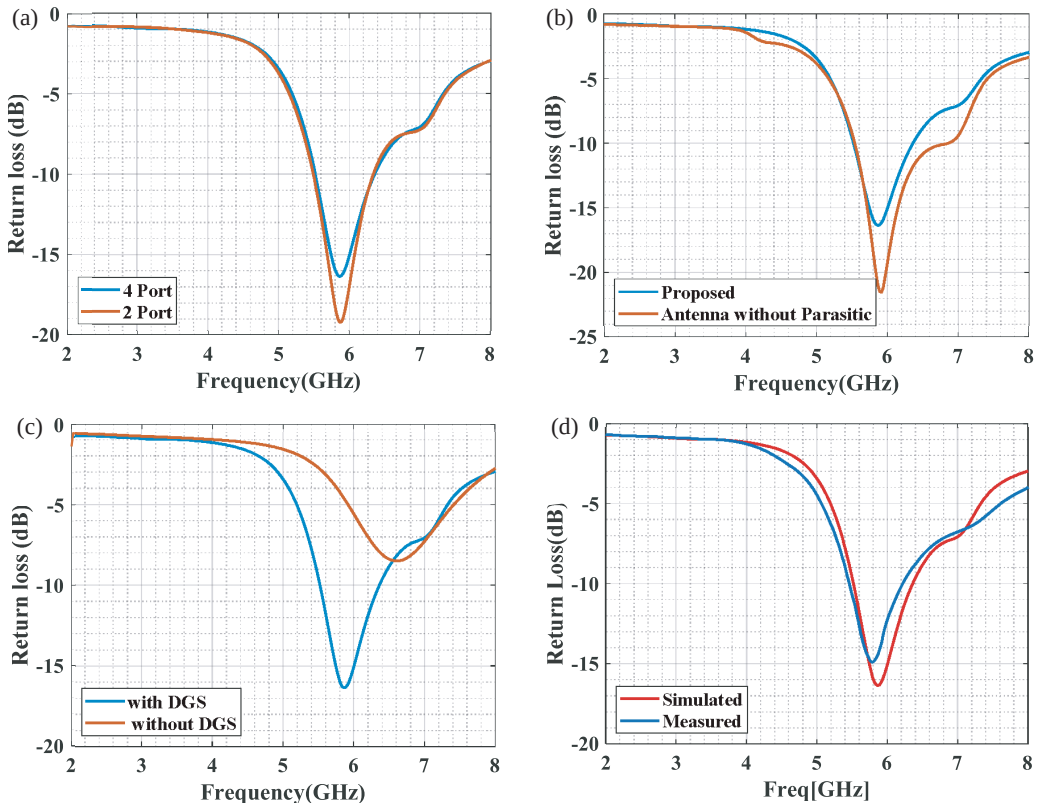

FIGURE 3. Return loss, (a) 4 ports, 2 ports, (b) with and without parasitic element, (c) with and without DGS, (d) measured and simulated results.

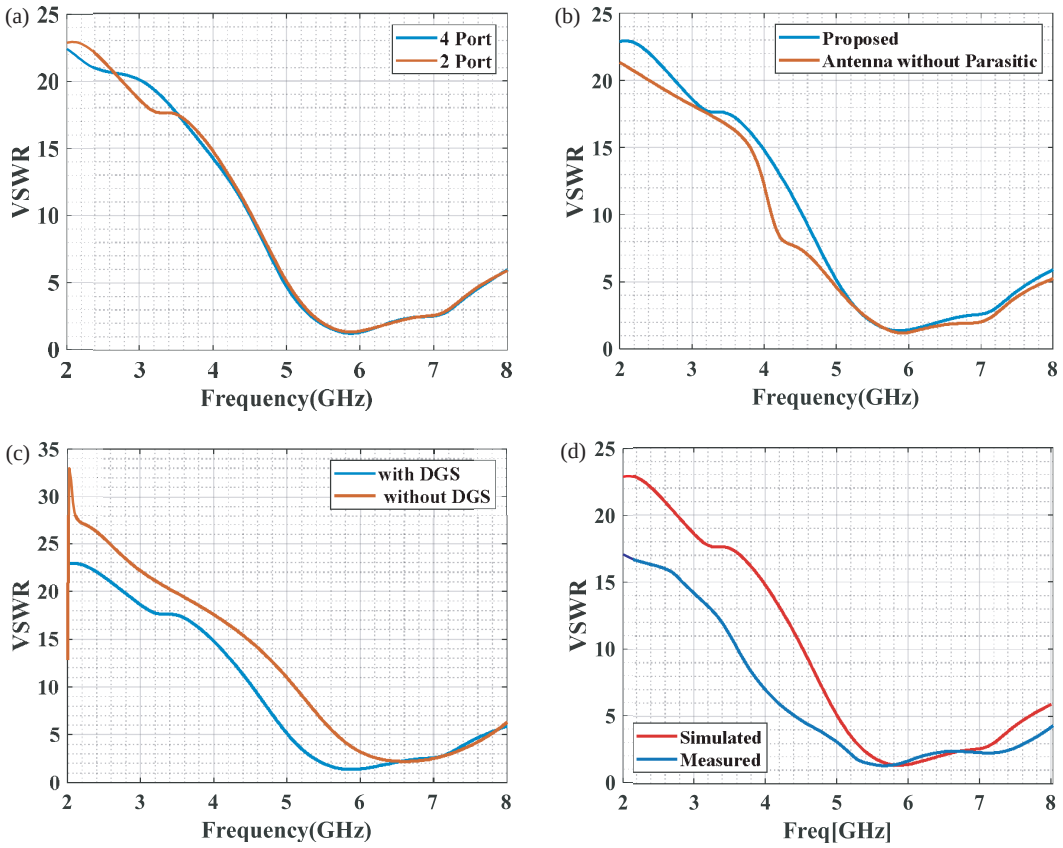

FIGURE 4. VSWR, (a) 4 ports, 2 ports, (b) with and without parasitic element, (c) with and without DGS, (d) measured and simulated results.

measured and simulated plots of return loss, which is almost similar.

VSWR: It is the representation of a total mismatch between the antenna and the feedline connecting to the antenna. The range of VSWR is between 1 and ∞, and values below 2 are said to be suitable for V2X communication. Figure 4 represents the VSWR of 4 ports, 2 ports, with and without parasitic element and with and without DGS, measured and simulated and parametric analysis. In Figures 4(a)–(c), the VSWR value of 2 port antenna is 1.1, without parasitic is 1.2, and without DGS is 2.3, and the proposed design achieved a better VSWR value of 1.0. Figure 4(d) shows the measured and simulated plots of VSWR, and the values of the simulated and measured VSWRs are almost similar.

Transmission coefficient: This measure is used to define the mutual coupling among the antenna elements. The transmission coefficient with and without parasitic patches is depicted in Figure 5. It is distinguished that the proposed design has very little mutual coupling (-28 dB) while using the parasitic patch. Further, the design without a parasitic patch achieved a transmission coefficient value of -18 dB. Thus, it can be demonstrated that using a parasitic patch decreased the mutual coupling among the antennas.

Radiation efficiency: This metric represents how the antennas are efficiently radiating and accepting the wave. It is the ratio that occurs between the radiated powers P_{rad} and input power P_s. It is expressed as:

$$Efficiency = \frac{P_{rad}}{P_s}\% \tag{10}$$

Figure 6(a) compares radiation efficiency with and without a parasitic patch. In this comparison, the achieved radiation efficiency is 96.9% with the parasitic patch and 96.6% without the parasitic patch for the operating frequency of 5.88 GHz. Figure 6(b) compares radiation efficiencies with and without a parasitic patch for all antennas excited simultaneously. In this comparison, the achieved radiation efficiency is 98.6% with the parasitic patch and 98.3% without the parasitic patch for the operating frequency of 5.88 GHz.

Radiation Pattern 2D and 3D: Radiation pattern depicts the antenna's radiation characteristics in a specific plane. Figures 7(a) and (b) show the 2D and 3D radiation patterns for the E-plane and H-plane at 5.88 GHz. Figure 7(a) shows the 2D measured and simulated radiation patterns. Figures 7(c) and (d) show the radiation patterns for co and cross polarizations without the parasitic element and the radiation pattern with the parasitic element.

Gain 2D and 3D: It specifically focuses on the magnitude of an antenna's transfer function, which relates the input signal to the output signal. This magnitude is usually expressed in decibels (dB). The gains of 2D and 3D for the proposed design are given in Figures 8(a) and (b). Figure 8(a) shows the 2D

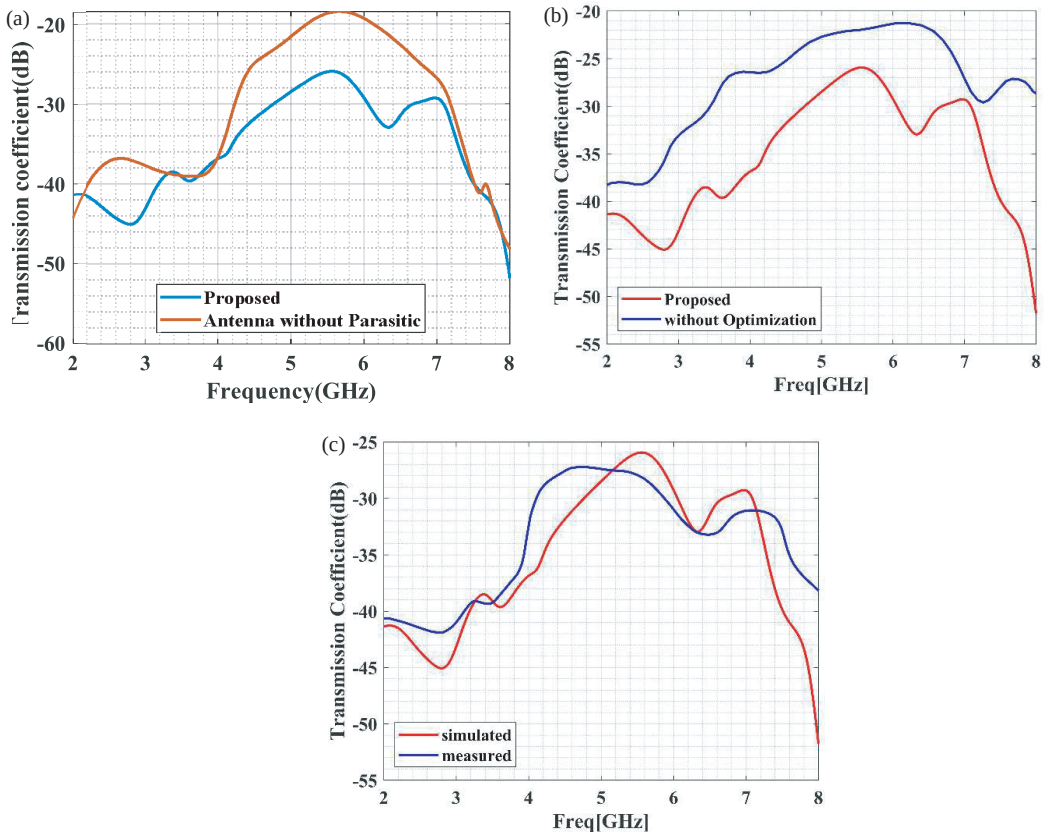

FIGURE 5. Transmission coefficient of the proposed design, (a) with and without parasitic design, (b) with and without optimization, (c) simulated and measured results.

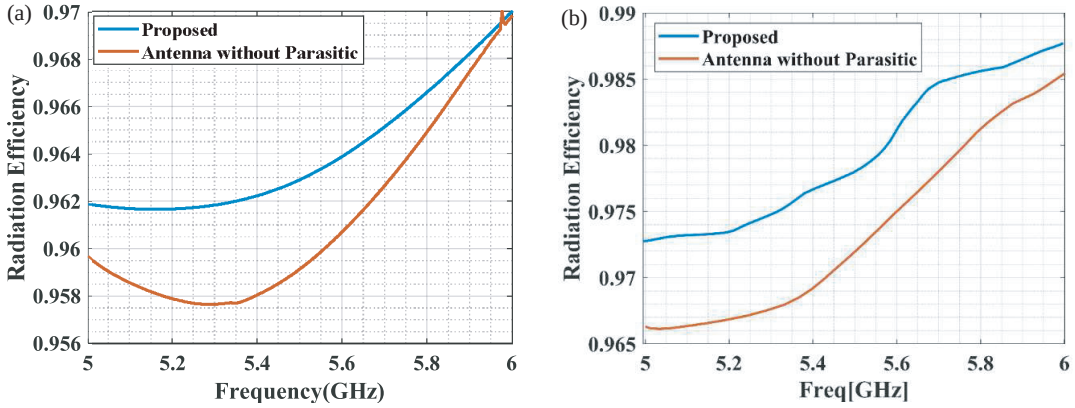

FIGURE 6. Comparison of radiation efficiency, (a) with and without parasitic, (b) all antenna excited simultaneously.

measured and simulated gains. The gain achieved by the proposed antenna is 9.7 dB. Figure 8(b) shows the 3D measured and simulated gains.

Surface Current Distribution (SCD): The electric current is generated by applying the electromagnetic field. Figure 9(a) shows the SCD of 2 ports, Figure 9(b) shows the SCD of 4 ports without parasitic patch, and Figure 9(c) shows the SCD of 4 ports with parasitic patch. The SCD is created in Figure 9 to examine the antenna's performance at its 5.88 GHz resonating frequency. As observed in Figure 9(a), the current flow is mainly seen at the edges of the antenna. Including a parasitic patch provides better resonance, and the current on the antenna surface dominates the entire radiation in Figure 9(b).

Co and Cross Polarization: In antenna design, co-polarization and cross-polarization refer to the orientation of the electric field (E-field) in the radio wave relative to a reference plane. This E-field orientation determines how effectively the antenna transmits or receives the signal. Figures 10(a) and (b) show the simulated and measured co and cross polarizations of the design.

Mutual Coupling: In MIMO antenna systems, mutual coupling refers to the unwanted electromagnetic interaction be-

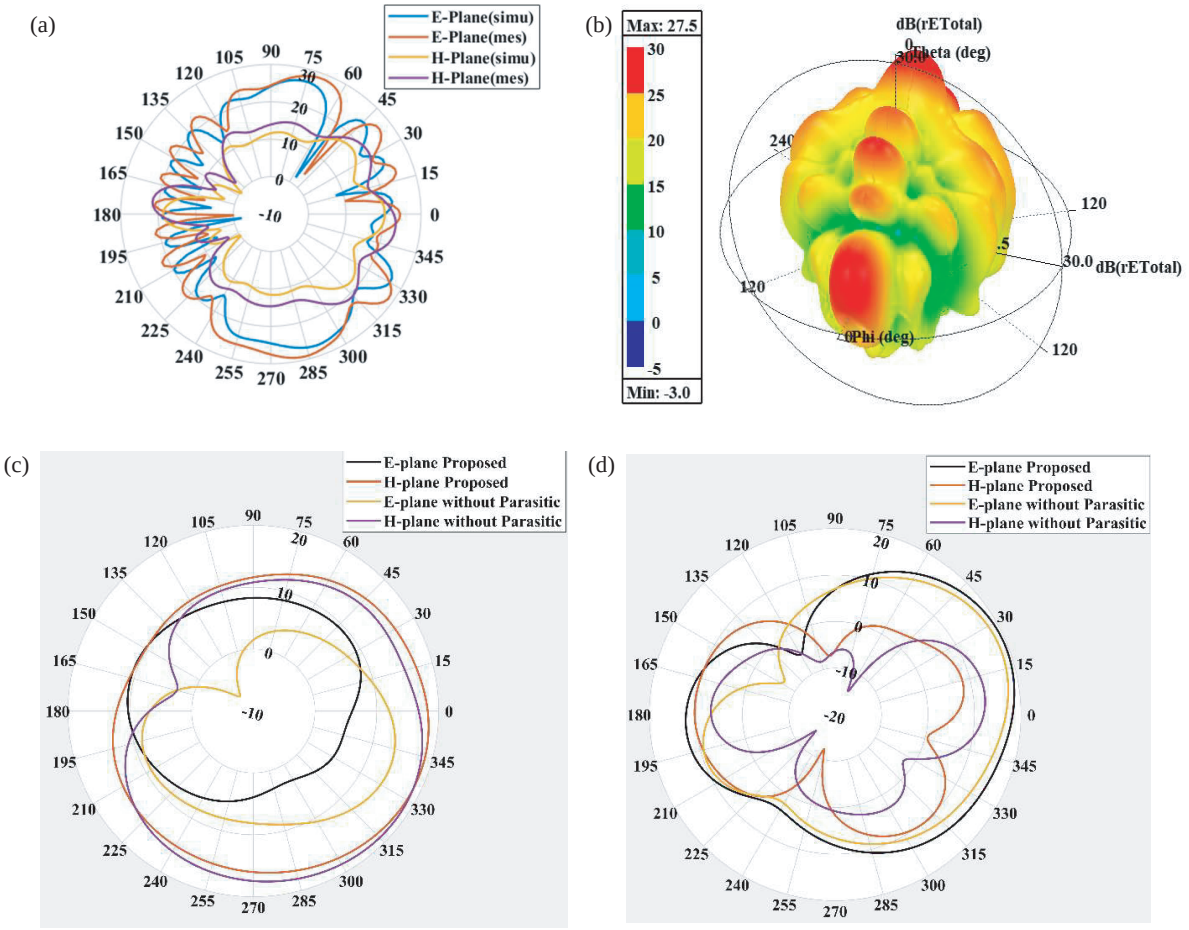

FIGURE 7. Radiation pattern, (a) 2D, (b) 3D, (c) Co polarization, and (d) Cross polarization.

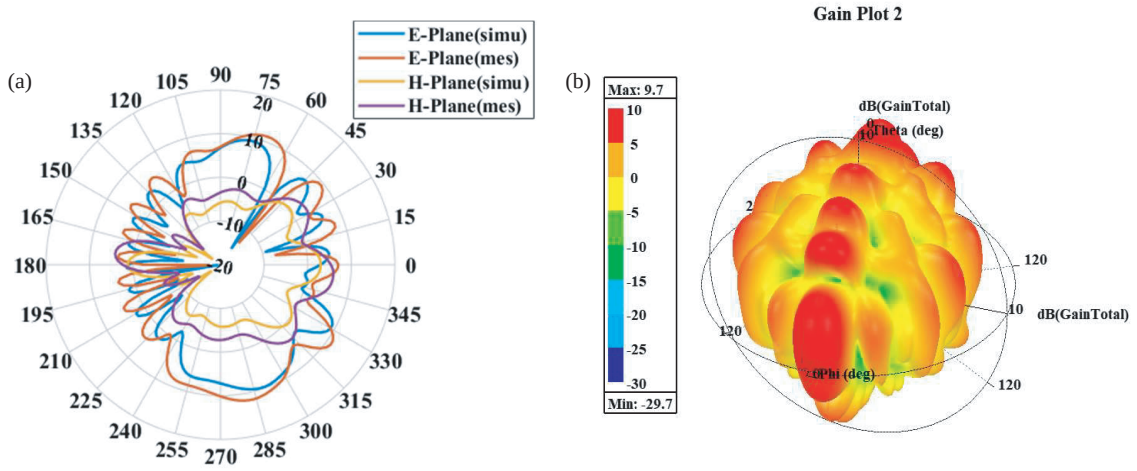

FIGURE 8. Gain, (a) 2D and (b) 3D.

tween the individual antenna elements. Figure 11 shows the mutual coupling of the antenna.

5.1. Analyzing the Performance of MIMO

This section presents the parameters of the MIMO antenna, like ECC, DG, TARC, MEG, and CCL, which are developed to validate the characteristics of MIMO antenna for multi-path propagation.

ECC: This metric shows how the individual elements in MIMO are based on radiation patterns and polarization. The squared value of the correlation-based coefficient is called ECC. That is, this measure presents the correlation among the radiation elements of the antenna. The ECC ρ_{ejk} of the de-

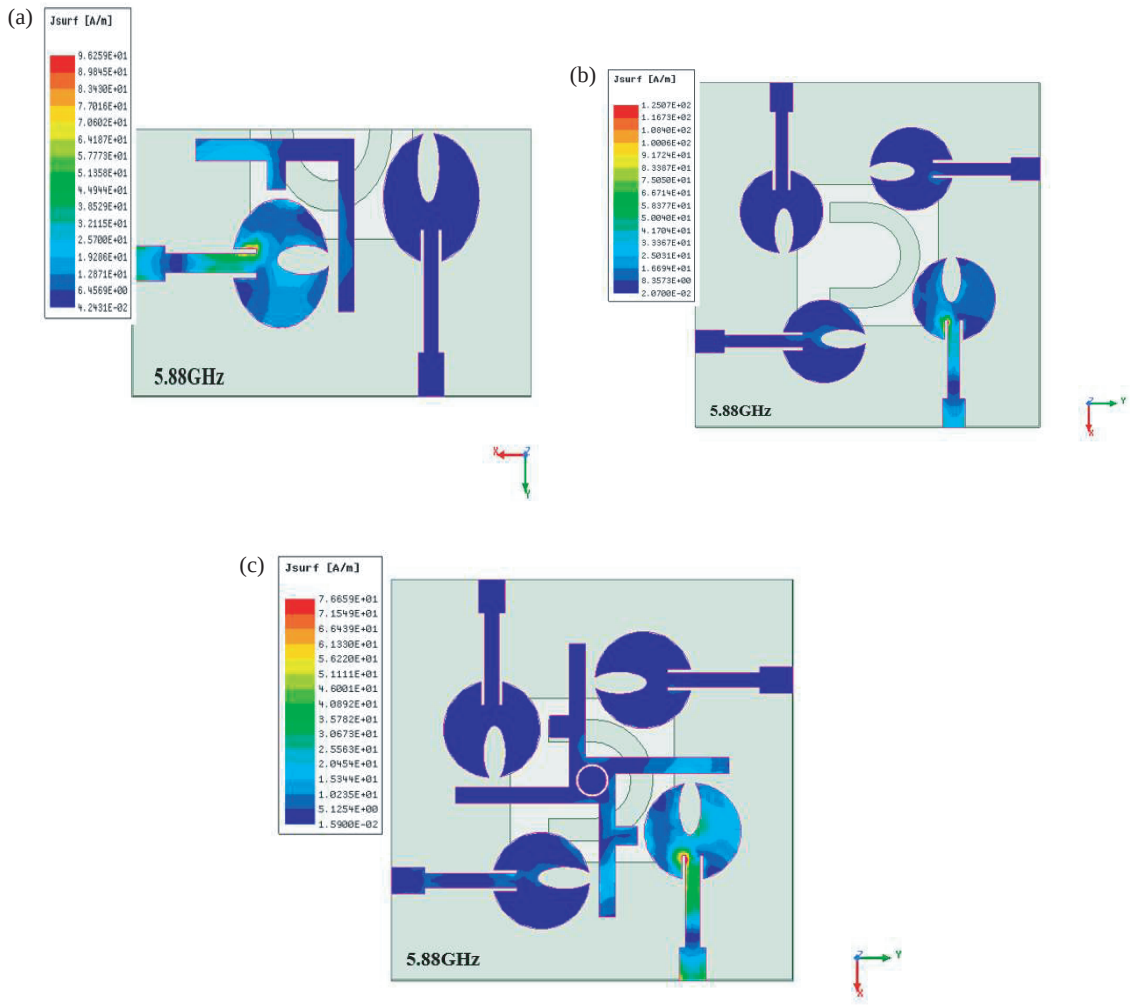

FIGURE 9. SCD of (a) 2 ports, (b) 4 ports without parasitic patch, and (c) 4 ports with parasitic patch.

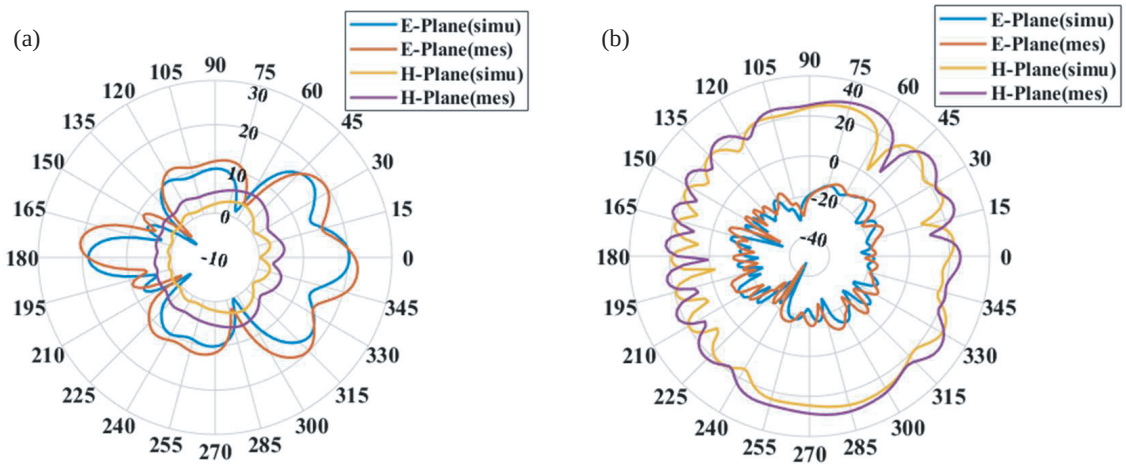

FIGURE 10. Simulated and measured (a) Co-polarization and (b) Cross-polarization.

veloped MIMO antenna model is measured based on far-field patterns and S-parameters. It is expressed as:

$$\rho_{ejk} = \frac{|S_{jj}S_{jk} + S_{kj}S_{kk}|^2}{(1-(|S_{jj}|^2+|S_{jk}|^2)+(1-|S_{kj}|^2+|S_{kk}|^2)} \quad (11)$$

$$\rho_{ejk} = \frac{|\iint_0^{4\pi} \left[\vec{R}_j(\theta,\phi)\vec{R}_k(\theta,\phi)\right] d\Omega|^2}{|\iint_0^{4\pi} \left[|\vec{R}_j(\theta,\phi)|^2 d\Omega \iint_0^{4\pi} |\vec{R}_k(\theta,\phi)|^2\right] d\Omega} \quad (12)$$

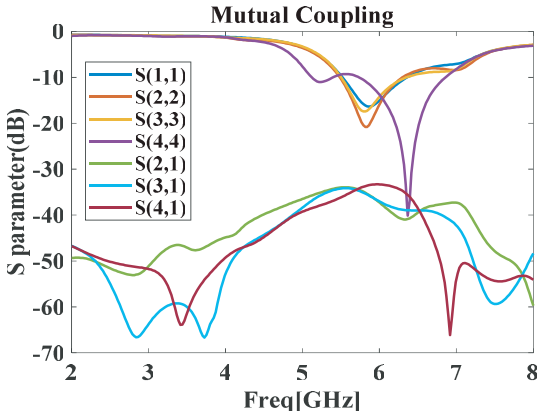

FIGURE 11. Mutual coupling.

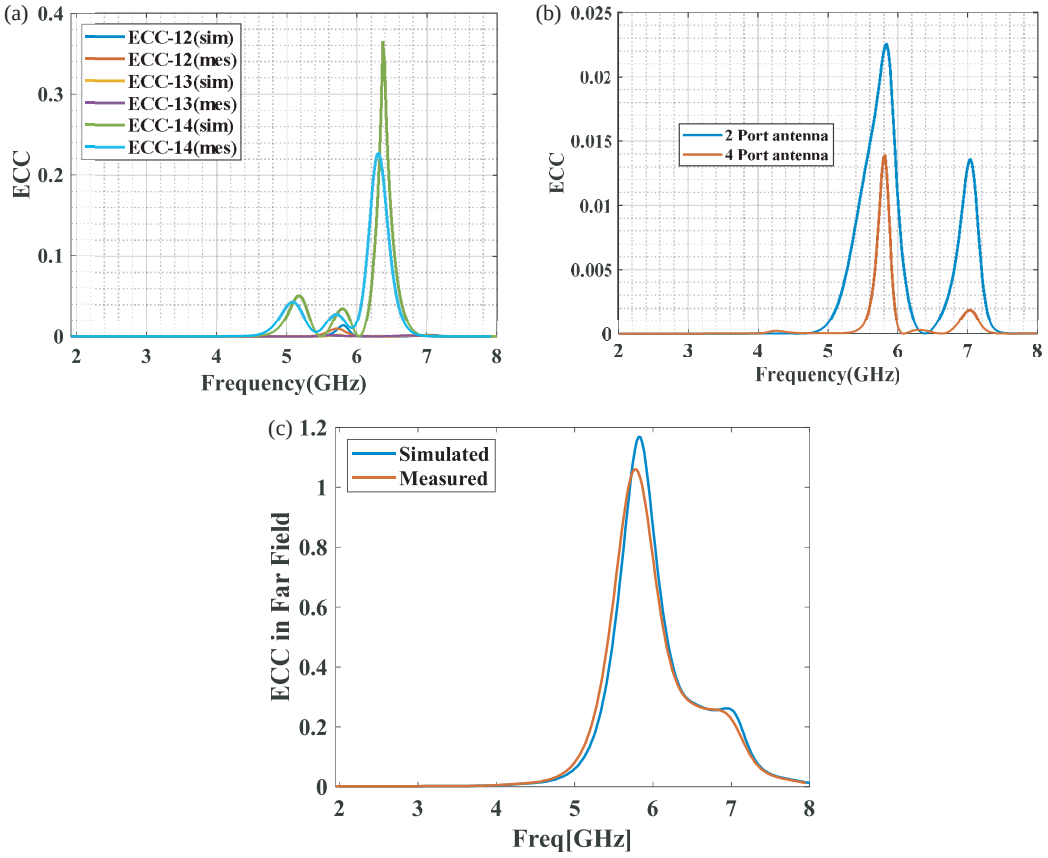

FIGURE 12. ECC of (a) simulated and measured by varying the ports, (b) 2 ports and 4 ports, (c) simulated and measured far fields.

where S_{jj} and S_{jk} are the return loss and transmission coefficient. $\vec{R}_j(\theta,\phi)$ and $\vec{R}_k(\theta,\phi)$ are the values of 3D radiation of the jth and kth antennas, and Ω is a solid angle. The ECC value is ideally considered to be 0, and practically, the acceptable range is (ECC < 0.5). The simulated and measured ECCs are given in Figure 12(a). The values of ECC attained for the proposed design (4 port) are about the range of 0.001 at the frequency of 5.88 GHz in Figure 12(a). However, the ECC value of 2 ports is greater than 0.013 in Figure 12(b). The simulated and measured far-field ECCs are given in Figure 12(c).

DG: For better reliability and quality in wireless communication systems, the DG value must be high, nearly 9.95 dB for the operating frequency. In the MIMO model, DG is defined as the incremental in-signal-to-interference stage. DG and ECC are interrelated; when DG's value is larger, ECC's value is less. DG is computed from the value of ECC through Equation (13).

$$DG = 10 \times \sqrt{1 - |\rho_{ejk}|^2} \tag{13}$$

Figure 13 presents the performance of DG by varying the ports. The performance of simulated and measured DGs is calculated

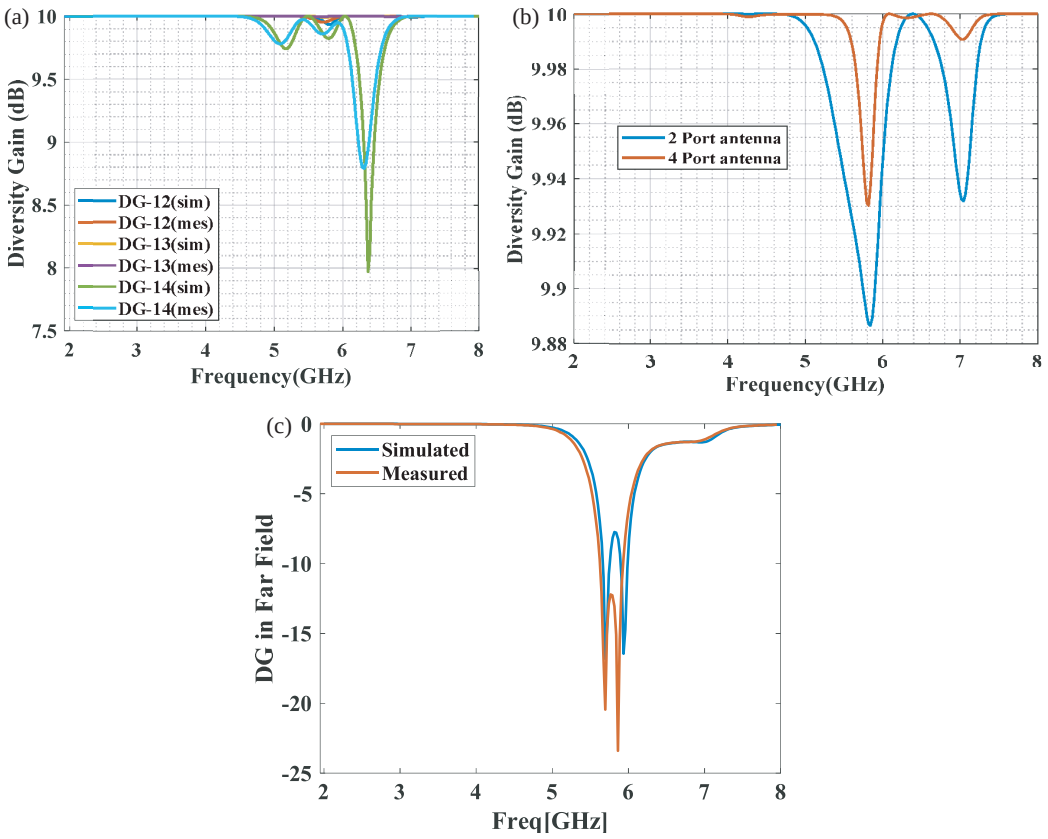

FIGURE 13. DG of (a) simulated and measured by varying the ports, (b) 2 ports and 4 ports, (c) simulated and measured far fields.

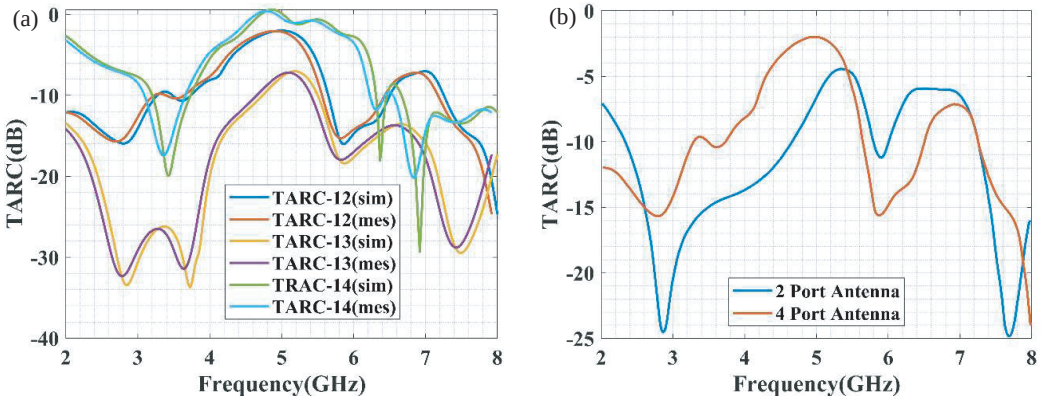

FIGURE 14. TARC of (a) simulated and measured by varying the ports, (b) 2 ports and 4 ports.

for ports 1 and 2, 1 and 3, and 1 and 4 in Figure 13(a). Similarly, the performance of DG is computed for the 2-port and 4-port antennas in Figure 13(b). Figure 13 shows that the DG value for both situations is roughly equivalent to 10 dB. The simulated and measured far-field DGs are given in Figure 13(c).

TARC: It is the essential diversity performance for better representation of MIMO antenna based on the resonating frequency and impedance bandwidth. It is the ratio of the square root of the total power incident to the total power reflected. For the specific phase angle among the excited ports of the antenna, the TARC focuses on all the S_{11} parameter details of the MIMO antenna.

$$TARC_{12} = \sqrt{|S_{11}+S_{12}e^{j\theta}|^2+|S_{22}+S_{21}e^{j\theta}|^2}/2 \quad (14)$$

$$TARC_{13} = \sqrt{|S_{11}+S_{13}e^{j\theta}|^2+|S_{33}+S_{31}e^{j\theta}|^2}/2 \quad (15)$$

$$TARC_{14} = \sqrt{|S_{11}+S_{14}e^{j\theta}|^2+|S_{44}+S_{41}e^{j\theta}|^2}/2 \quad (16)$$

where θ defines the excitation phase angle.

Figure 14 presents the performance of TARC by varying the ports. The performance of simulated and measured TARCs is calculated for ports 1 and 2, 1 and 3, and 1 and 4 in Figure 14(a).

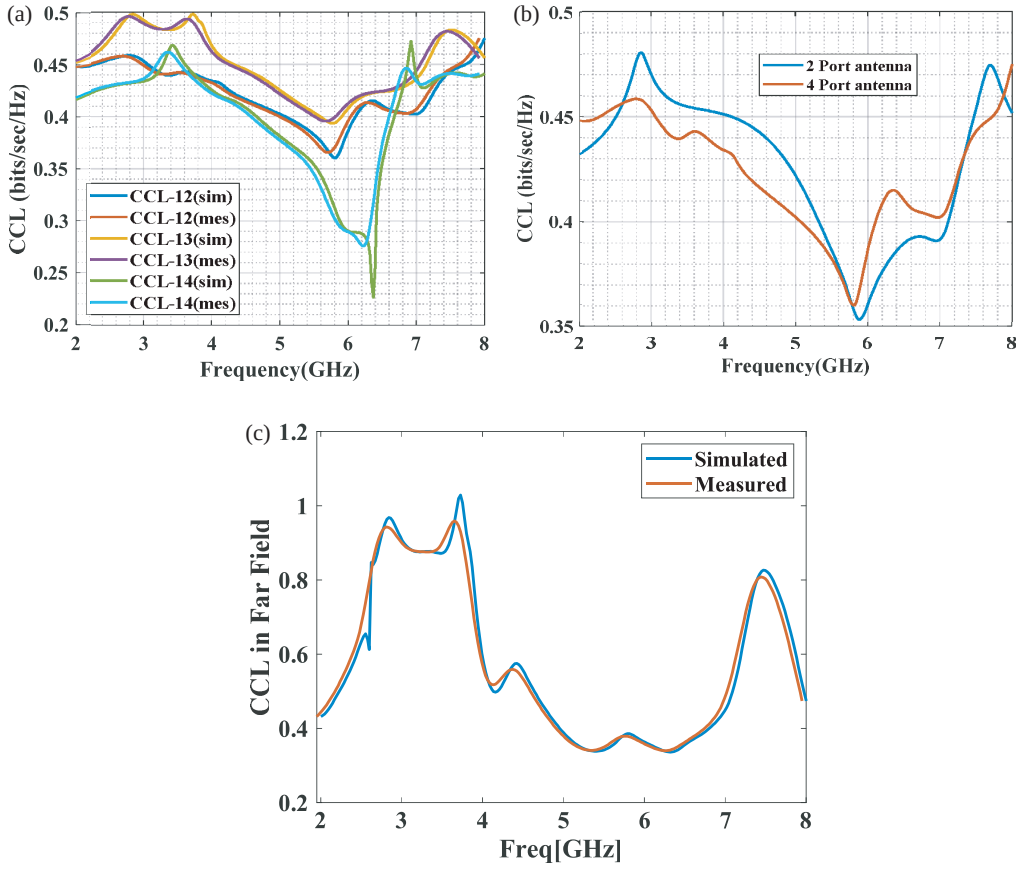

FIGURE 15. CCL of (a) simulated and measured ones by varying the ports, (b) 2 ports and 4 ports, (c) simulated and measured far fields.

Similarly, the performance of TARC is computed for the 2-port and 4-port antennas in Figure 14(b). It can be seen that the TARC value for 4 port antenna is -46 dB, and that for 2 port antenna is -42 dB.

CCL: This metric details the MIMO model's CCL on the correlation effect. It defines the large quantity of channel loss that permits the data to be better transmitted on the communication channels. For better communication, the CCL value should not be higher than 0.4 bits/s/Hz. To find the CCL value, the following expressions are used.

$$C(loss) = -\log_2 \det(f) \tag{17}$$

$$f = \begin{bmatrix} \rho e_{11} & \rho e_{12} \\ \rho e_{21} & \rho e_{22} \end{bmatrix} \tag{18}$$

where f is the matrix of correlation.

$$\sigma_{ii} = 1 - \left(|S_{ii}|^2 - |S_{ij}|^2\right) \tag{19}$$

$$\sigma_{ij} = -\left(S_{ii}^* S_{ij} + S_{ji} S_{jj}^*\right) \tag{20}$$

Figure 15 indicates the performance of CCL for 2-port and 4-port MIMO antennas. The performance of the CCL value is simulated and measured for ports 1 and 2, 1 and 3, and 1 and 4, which is shown in Figure 15(a). Similarly, the performance of CCL is computed for the 2-port and 4-port antennas in Figure 15(b). It can be seen that the CCL value is fewer than 0.4 bits/s/Hz. This performance shows that the proposed MIMO antenna is more adaptable for V2X applications. The CCLs of the simulated and measured far field plots are given in Figure 15(c).

Channel Capacity: To calculate the channel capacity represented as C, the estimation relies on the utilization of Equation (21),

$$C = E\left\{\log_2\left[\det\left(I + \frac{SNR}{\eta_T} H H^H\right)\right]\right\} \tag{21}$$

where the variable I represents the identity matrix, E the bandwidth, η_T the number of antennas at the transmitter side, SNR

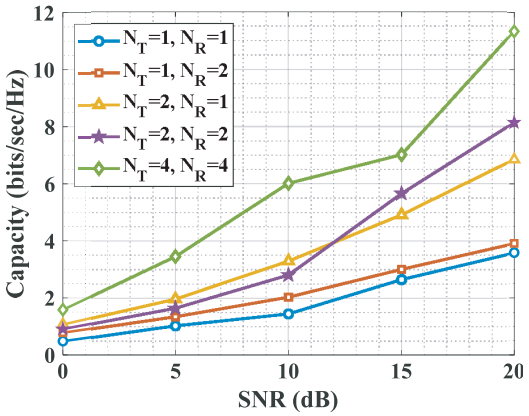

FIGURE 16. Channel capacity.

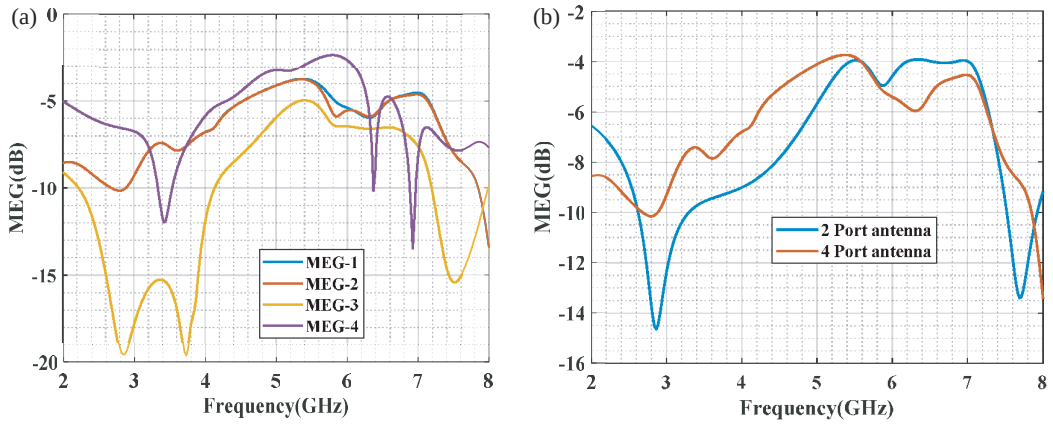

FIGURE 17. MEG of (a) by varying the ports, (b) 2 port and 4 port.

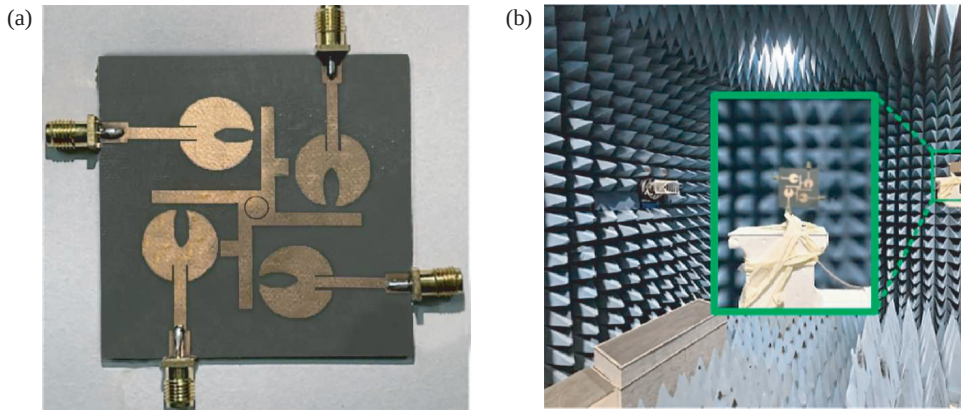

FIGURE 18. Fabricated design, (a) 4-port MIMO design and (b) tested with anechoic chamber.

the signal to noise ratio, and H^H the Hermitian transpose, respectively. Figure 16 shows the channel capacity plot.

MEG: It is an essential performance in the MIMO antenna, and it is the rate of power accepted in the antenna's diversity to power attained in an omnidirectional antenna. It defines the MIMO antenna's gain performance. Figure 17 shows the MEG performance of a proposed design in all four ports. The value of MEG is computed using S-the parameter by the following expression:

$$MEG_i = 0.5\mu_{irad} = 0.5\left(1 - \sum_{ij}^{N} |S_{ij}|\right) \quad (22)$$

$$l = |MEG_1 - MEG_2| < 3\,\text{dB} \quad (23)$$

where l is the ratio of power and the variation in MEG magnitude; N is the total antennas; i, j are the elements of an antenna; and μ_{irad} is the radiation efficiency. For better diversity performances of the antenna, the standard value of MEG is considered to be $-3 \leq |MEG\,(\text{dB}) < -12$. Figure 17 shows that the MEG value of the 4-port is found to be -3 dB at the resonating frequency of 5.88 dB.

A fabricated 4-port MIMO antenna is successfully designed and validated for the desired performance with the help of a vector network analyser. The antenna was fabricated on an FR4 substrate, and the measurements were performed to endorse the antenna's capabilities. Figure 18(a) shows the 4-port MIMO fabricated prototype antenna design. The antenna is tested and measured in an anechoic chamber, which is given in Figure 18(b).

5.2. Discussion

In existing research works, various antennas designed have been proposed for V2X applications and some other wireless applications. Some of the antenna designs are like single patch, monopole antenna, and conventional MIMO. These models have some issues like limited diversity performances which lead to reducing the performances in dense urban environments. Some of the recent research works such as CPW assisted MIMO antenna [18], four-port CP MIMO antenna [20], and maze-shaped asymmetric antenna [24] have contributed to the design of MIMO antennas for various applications. These antenna models have obtained minimum depth in return loss, low radiation efficiency, low isolation, and high mutual coupling issues. The proposed antenna has been measured with various parameters, which have been obtained with the values nearest to -18 dB at the resonating frequency of 5.88 GHz. This antenna model has obtained enhanced radiation efficiency of greater than 97% and isolation values of less than -25 dB com-

TABLE 3. Performance comparison of the various designs.

Authors	Ports	Frequency (GHz)	Electrical Dimension	Size (mm)	Return loss (− dB)	efficiency
Sujanth Narayan et al. [18]	4	5.8	-	$60 \times 60 \times 1.6$	< -10 dB	60%–80%
Sufian et al. [20]	4	5.9	$1.4\lambda_0 \times 1.4\lambda_0 \times 0.03\lambda_0$	$74 \times 74 \times 0.508$	< -20 dB	94%
Feng et al. [28]	4	5.82	-	$76 \times 76 \times 17$	< -20 dB	-
Yacoub et al. [29]	2	5.9	-	60×38.5	-	85%
Kumar et al. [30]	4	2.53 to 7.3	$0.5\lambda_0 \times 0.7\lambda_0$	-	-	-
Kumar et al. [31]	2	4.27 to 10.1	$0.42\lambda_0 \times 0.28\lambda_0$	$30 \times 20 \times 1.6$	< -20 dB	90%
Kumar et al. [32]	2	2.83 to 7.21	$0.44\lambda_0 \times 0.35\lambda_0$	47.7×38	< -20 dB	92%
Mahto et al. [33]	4	2.42 to 7.45	$0.28\lambda_0 \times 0.28\lambda_0$	$35 \times 35 \times 1.6$	< -20 dB	90%
Singh et al. [34]	2	7.2 to 8.9	-	$10.6 \times 10.3 \times 1.6$	< -20 dB	69.2%
Mistri et al. [38]	4	23.56–28.25 GHz	-	$35 \times 35 \times 0.76$	< -20 dB	92%
Singh et al. [40]	4	3.35–5.73	$0.45\lambda_0 \times 0.45\lambda_0$	-	< -10 dB	85%
Proposed	**4**	**5.88**	**-**	$\mathbf{73.2 \times 73.3 \times 0.508}$	$< \mathbf{-20}$ dB	**97.9%**

pared to the compared models. The proposed four-port circular patch MIMO antenna with U-shaped DGS and F-shaped parasitic stubs addresses the limitations found in existing antenna designs for V2X communication, including mutual coupling, reduced gain, and poor isolation. By incorporating innovative design elements and optimizing parameters through an AO optimization algorithm, the antenna achieves notable improvements, such as enhanced radiation efficiency exceeding 97%, isolation values below -25 dB, and a return loss near -18 dB at 5.88 GHz. Its potential applications in V2X communication systems include enhancing vehicle-to-vehicle and vehicle-to-infrastructure interactions, and supporting more reliable and efficient smart transportation systems. Table 3 presents the performance comparison of various designs based on V2X communication applications. Here, all the designs are operated at a frequency of 5.8 to 5.9. The proposed design has achieved a better radiation efficiency of 96.9% than existing works.

6. CONCLUSION

This work has presented a 4-port high-gain MIMO antenna for V2X communications. Here, parasitic patch and DGS are used to increase the gain of the MIMO model. This design has a compact size of $73.2 \times 73.3 \times 0.508\,\text{mm}^3$ and resonates at 5.88 GHz. In this work, U-shaped DGS and F-shaped parasitic patches are introduced to reduce the mutual coupling among the antenna elements. Transmission coefficient is used to show the performance of mutual coupling. The suggested design has less mutual coupling (-28 dB) while considering the parasitic patch and achieved -18 dB without the parasitic patch. Further, diversity performances such as CCL, MEG, TARC, ECC, and DG are used to define the 4-port MIMO performance. The proposed design satisfied all criteria and finally proved that it is well suited for V2X communication. However, the Aquila optimization algorithm faced limited exploration-exploitation balance and slow convergence, which can lead to increased simulation time and computational cost. In the future, the proposed simulated design will be fabricated using sophisticated high convergence optimization, and the operational characteristics of a simulated and fabricated MIMO system will be contrasted.

REFERENCES

[1] Aminu-Baba, M., M. K. A. Rahim, F. Zubir, A. Y. Iliyasu, K. I. Jahun, M. F. M. Yusoff, M. M. Gajibo, A. A. Pramudita, and I. K. C. Lin, "A compact triband miniaturized MIMO antenna for WLAN applications," *AEU — International Journal of Electronics and Communications*, Vol. 136, 153767, 2021.

[2] BharathiDevi, B. and J. Kumar, "Small frequency range discrete bandwidth tunable multiband MIMO antenna for radio/LTE/ISM-2.4 GHz band applications," *AEU — International Journal of Electronics and Communications*, Vol. 144, 154060, 2022.

[3] Kumar, A., "Compact 4 x 4 CPW-fed MIMO antenna with Wi-Fi and WLAN notch for UWB applications," *Radioelectronics and Communications Systems*, Vol. 64, No. 2, 92–98, 2021.

[4] Singh, D., S. D. Choudhary, and B. Mohapatra, "Design of microstrip patch antenna for Ka-band (26.5–40 GHz) applications," *Materials Today: Proceedings*, Vol. 45, 2828–2832, 2021.

[5] Triwinarko, A., I. Dayoub, and S. Cherkaoui, "PHY layer enhancements for next generation V2X communication," *Vehicular Communications*, Vol. 32, 100385, 2021.

[6] Shi, Y., Q. Han, W. Shen, and X. Wang, "A multi-layer collaboration framework for industrial parks with 5G vehicle-to-everything networks," *Engineering*, Vol. 7, No. 6, 818–831, 2021.

[7] Rasheed, I., L. Zhang, and F. Hu, "A privacy preserving scheme for vehicle-to-everything communications using 5G mobile edge computing," *Computer Networks*, Vol. 176, 107283, 2020.

[8] Kaushik, D., A. Gupta, and e. al., "WITHDRAWN: Ultra-secure transmissions for 5G-V2X communications," Materials Today: Proceedings, 2021.

[9] Tran, H. H., N. Hussain, and T. T. Le, "Low-profile wideband circularly polarized MIMO antenna with polarization diversity for WLAN applications," *AEU — International Journal of Electronics and Communications*, Vol. 108, 172–180, 2019.

[10] Dwivedi, A. K., A. Sharma, A. K. Singh, and V. Singh, "Metamaterial inspired dielectric resonator MIMO antenna for isolation enhancement and linear to circular polarization of waves," *Measurement*, Vol. 182, 109681, 2021.

[11] Yon, H., N. H. A. Rahman, M. A. Aris, M. H. Jamaluddin, I. K. C. Lin, H. Jumaat, F. N. M. Redzwan, and Y. Yamada, "Development of C-shaped parasitic MIMO antennas for mutual coupling reduction," *Electronics*, Vol. 10, No. 19, 2431, 2021.

[12] Babu, K. V. and B. Anuradha, "Design of UWB MIMO antenna to reduce the mutual coupling using defected ground structure," *Wireless Personal Communications*, Vol. 118, No. 4, 3469–3484, 2021.

[13] Niu, Z., H. Zhang, Q. Chen, and T. Zhong, "Isolation enhancement in closely coupled dual-band MIMO patch antennas," *IEEE Antennas and Wireless Propagation Letters*, Vol. 18, No. 8, 1686–1690, 2019.

[14] Soltani, S., P. Lotfi, and R. D. Murch, "A dual-band multiport MIMO slot antenna for WLAN applications," *IEEE Antennas and Wireless Propagation Letters*, Vol. 16, 529–532, 2016.

[15] Jiang, W., B. Liu, Y. Cui, and W. Hu, "High-isolation eight-element MIMO array for 5G smartphone applications," *IEEE Access*, Vol. 7, 34 104–34 112, 2019.

[16] Lee, W.-W. and Y.-S. Cho, "A high-isolation mimo antenna with dual-feed structure for WiFi of mobile phones," *Microwave and Optical Technology Letters*, Vol. 59, No. 4, 930–934, 2017.

[17] Deng, J., J. Li, L. Zhao, and L. Guo, "A dual-band inverted-F MIMO antenna with enhanced isolation for WLAN applications," *IEEE Antennas and Wireless Propagation Letters*, Vol. 16, 2270–2273, 2017.

[18] Sujanth Narayan, K. G., J. A. Baskaradas, and D. R. Kumar, "Design of a CPW-fed compact MIMO antenna for next generation vehicle to everything (V2X) communication," *Wireless Personal Communications*, Vol. 120, No. 3, 2179–2200, 2021.

[19] Ishfaq, M. K., S. A. Babale, H. T. Chattha, M. Himdi, A. Raza, M. Younas, T. A. Rahman, S. K. A. Rahim, and B. A. Khawaja, "Compact wide-angle scanning multibeam antenna array for V2X communications," *IEEE Antennas and Wireless Propagation Letters*, Vol. 20, No. 11, 2141–2145, 2021.

[20] Sufian, M. A., N. Hussain, A. Abbas, J. Lee, S. G. Park, and N. Kim, "Mutual coupling reduction of a circularly polarized MIMO antenna using parasitic elements and DGS for V2X communications," *IEEE Access*, Vol. 10, 56 388–56 400, 2022.

[21] Ko, M., H. Lee, and J. Choi, "Planar LTE/sub-6 GHz 5G MIMO antenna integrated with mmwave 5G beamforming phased array antennas for V2X applications," *IET Microwaves, Antennas & Propagation*, Vol. 14, No. 11, 1283–1295, 2020.

[22] Ali, W. A. E., M. I. Ashraf, and M. A. Salamin, "A dual-mode double-sided 4 × 4 MIMO slot antenna with distinct isolation for WLAN/WiMAX applications," *Microsystem Technologies*, Vol. 27, No. 3, 967–983, 2021.

[23] Dwivedi, A. K., A. Sharma, A. K. Pandey, and V. Singh, "Two port circularly polarized MIMO antenna design and investigation for 5G communication systems," *Wireless Personal Communications*, Vol. 120, No. 3, 2085–2099, 2021.

[24] Naidu, P. V., M. B. Dhanekula, K. M. Almustafa, A. Kumar, K. A. Meerja, and S. H. Akkapanthula, "Design and performance analysis of MAZE shaped quad port ACS fed tri band MIMO antenna for V2V and multi band applications," *AEU — International Journal of Electronics and Communications*, Vol. 134, 153676, 2021.

[25] Sharma, P. K., J. R. Szymański, M. Żurek Mortka, M. Sathiyanarayanan, and D. Sharma, "Design and analysis of four leaf clover shaped MIMO antenna for Sub-6 GHz V2X applications," *Frequenz*, Vol. 78, No. 7-8, 2024.

[26] Aliqab, K., A. Armghan, M. Alsharari, and M. H. Aly, "Highly decoupled and high gain conformal two-port MIMO antenna for V2X communications," *Alexandria Engineering Journal*, Vol. 74, 599–610, 2023.

[27] Abualigah, L., D. Yousri, M. A. Elaziz, A. A. Ewees, M. A. A. Al-Qaness, and A. H. Gandomi, "Aquila optimizer: A novel meta-heuristic optimization algorithm," *Computers & Industrial Engineering*, Vol. 157, 107250, 2021.

[28] Feng, B., J. Chen, S. Yin, C.-Y.-D. Sim, and Z. Zhao, "A tripolarized antenna with diverse radiation characteristics for 5G and V2X communications," *IEEE Transactions on Vehicular Technology*, Vol. 69, No. 9, 10 115–10 126, 2020.

[29] Yacoub, A., M. Khalifa, and D. N. Aloi, "Compact 2 × 2 automotive MIMO antenna systems for sub-6 GHz 5G and V2X communications," *Progress In Electromagnetics Research B*, Vol. 93, 23–46, 2021.

[30] Kumar, P., R. Sinha, A. Choubey, and S. K. Mahto, "A novel metamaterial electromagnetic band gap (MM-EBG) isolator to reduce mutual coupling in low-profile MIMO antenna," *Journal of Electronic Materials*, Vol. 51, No. 2, 626–634, 2022.

[31] Kumar, P., R. Sinha, A. Choubey, and S. K. Mahto, "DGS based miniaturized wideband MIMO antenna with efficient isolation for C band applications," *Frequenz*, Vol. 77, No. 3-4, 163–172, 2023.

[32] Kumar, P., A. K. Singh, R. Kumar, S. K. Mahto, P. Pal, R. Sinha, A. Choubey, and A. J. A. Al-Gburi, "Design and analysis of low profile stepped feedline with dual circular patch MIMO antenna and stub loaded partial ground plane for wireless applications," *Progress In Electromagnetics Research C*, Vol. 140, 135–144, 2024.

[33] Mahto, S. K., A. K. Singh, R. Sinha, M. Alibakhshikenari, S. Khan, and G. Pau, "High isolated four element MIMO antenna for ISM/LTE/5G (sub-6 GHz) applications," *IEEE Access*, Vol. 11, 82 946–82 959, 2023.

[34] Singh, A. K., S. K. Mahto, and R. Sinha, "A miniaturized MIMO antenna for C, X, and Ku band applications," *Progress In Electromagnetics Research C*, Vol. 117, 31–40, 2021.

[35] Singh, A. K., S. K. Mahto, and R. Sinha, "Compact super-wideband MIMO antenna with improved isolation for wireless communications," *Frequenz*, Vol. 75, No. 9-10, 407–417, 2021.

[36] Kumar, P., R. Sinha, A. Choubey, and S. K. Mahto, "A miniaturized rectangular shape narrowband MIMO antenna with reduced mutual coupling for C-band applications," *J. Electromagn. Waves Appl.*, Vol. 36, No. 12, 1717–1730, 2022.

[37] Singh, A. K., S. K. Mahto, and R. a. Sinha, "Circular shape dual element MIMO antenna for 5G (sub-6 GHz) application," in *2022 IEEE Microwaves, Antennas, and Propagation Conference (MAPCON)*, 583–587, Bangalore, India, Dec. 2022.

[38] Mistri, R. K., A. K. Singh, S. K. Mahto, and R. Sinha, "Quad element millimetrewave MIMO antenna for 5G communication," *Journal of Electromagnetic Waves and Applications*, Vol. 37, No. 15, 1258–1273, 2023.

[39] Singh, A. K., S. K. Mahto, and R. Sinha, "Dual element MIMO antenna with improved radiation efficiency for 5G millimeter-wave applications," in *2022 IEEE Region 10 Symposium (TENSYMP)*, 1–5, Mumbai, India, Jul. 2022.

[40] Singh, A. K., S. K. Mahto, and R. Sinha, "Quad element MIMO antenna for LTE/5G (sub-6 GHz) applications," *Journal of Elec-*

tromagnetic Waves and Applications, Vol. 36, No. 16, 2357–2372, 2022.

[41] Singh, A. K., S. K. Mahto, P. Kumar, R. K. Mistri, and R. Sinha, "Reconfigurable circular patch MIMO antenna for 5G (sub-6 GHz) and WLAN applications," in *International Journal of Communication Systems*, Vol. 35, No. 16, e5313, 2022.

[42] Singh, A. K., S. K. Mahto, and R. Sinha, "Reconfigurable dual element dual band MIMO antenna for 5G (sub-6 GHz) and WLAN applications," *COMPEL — The International Journal for Computation and Mathematics in Electrical and Electronic Engineering*, Vol. 41, No. 5, 1940–1955, 2022.